energy&fuels

pubs.acs.org/EF
Article

Pressurized Gasification of Beech Wood Char in Steam and Steam–CO_2 Mixtures: Kinetics Considering Steam–CO_2 Interaction

Stella Walker* and Thomas Kolb

Cite This: https://doi.org/10.1021/acs.energyfuels.5c04287
Read Online

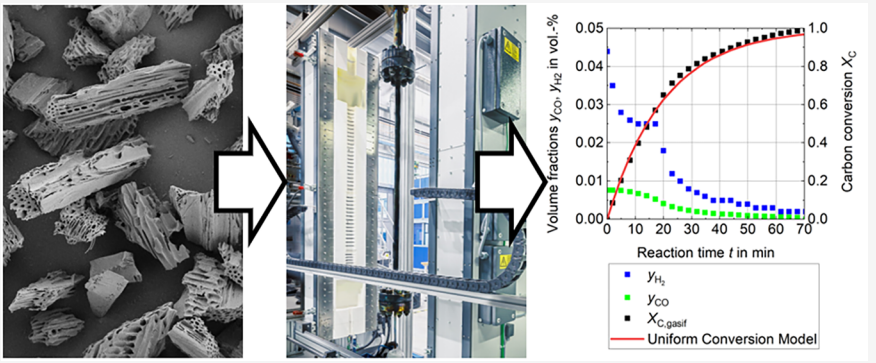

ABSTRACT: High-quality, tar-free syngas can be produced from lignocellulosic and low-grade biogenic feedstocks via pressurized entrained flow gasification. However, the gasification behavior of biomass char in typical atmospheres of mixtures of H_2O and CO_2 at partial pressures of about 10 bar each has not been investigated so far. The work at hand therefore presents experimental and kinetic modeling results of beech wood char gasification in H_2O at partial pressures of up to 12.5 bar and in mixtures of H_2O and CO_2 at various partial pressure combinations at a total pressure of 20 bar. Two char qualities are investigated that vary with respect to their micropore surface area, degree of graphitization, and dispersion of calcium. The gasification kinetics in steam are described with a power law and a Langmuir–Hinshelwood model. In a H_2O atmosphere, the power law model provides good fitting accuracy. Together with CO_2 kinetics published in an earlier work, the theoretical expressions for additive and competitive behavior are formulated. While the additive mechanism adds the H_2O and CO_2 kinetics, the competitive mechanism combines the rate constants of the Langmuir–Hinshelwood kinetics in H_2O and CO_2 atmospheres in one expression. The theoretical approaches are compared to the experimentally derived kinetics in a mixture of H_2O and CO_2. For both chars, a transition from additive to competitive behavior is observed with increasing partial pressures. Experiments indicate that especially the degree of graphitization and therefore the severity of heat treatment during pyrolysis strongly impact the transition from additive to competitive behavior of H_2O and CO_2. With higher degrees of graphitization, the transition occurs at lower H_2O and CO_2 partial pressures. Interestingly, synergistic behavior can be observed in a small range of partial pressures and explained by the positive effect of steam on the dispersion of calcium, which, in turn, catalyzes the Boudouard reaction.

1. INTRODUCTION

Entrained flow gasification (EFG) is a pathway to convert carbon-based feedstock to synthesis gas, a starting point for the synthesis of liquid and gaseous fuels and base chemicals. For low-grade biogenic or anthropogenic wastes, a combination of pyrolysis followed by EFG can be an important element of a circular economy.[1]

In the case of biogenic feedstock, a suspension of pyrolysis char particles in the size range of 100 μm and pyrolysis oil is atomized into the entrained flow reactor and reacts with steam and oxygen at pressures of up to 40 bar. The conversion to the synthesis gas consists of parallel and subsequent process steps. In the flame zone, oxygen reacts with recirculating syngas, creating high local temperatures of more than 1800 °C. At these temperatures, the suspension fuel droplets undergo drying and evaporation, cracking of tars, and secondary pyrolysis of char particles. The flame is surrounded by an oxygen-free atmosphere where the char particles are converted to synthesis gas in heterogeneous gasification reactions.[2,3] The latter is a slow and, therefore, a rate-determining step. The gasification reactions are the Boudouard reaction 1 and heterogeneous water–gas reaction 2

Received: August 14, 2025
Revised: November 7, 2025
Accepted: November 7, 2025

$$C + CO_2 \rightarrow 2CO \quad (1)$$

$$C + H_2O \rightarrow H_2 + CO \quad (2)$$

For the design and operation of EFG plants, especially the influence of the reaction gas composition and partial pressures on the reaction rate and therefore the particle conversion is of great importance. H_2O and CO_2 may react with the carbon atoms on the char surface independently from one another or compete for reactive sites. The interaction of both molecules strongly affects the resulting reaction rate. It is therefore crucial to carry out gasification experiments in mixed atmosphere at technically relevant partial pressures. In EFG reactors, the partial pressures of the gasifying agents H_2O and CO_2 both lie in the range of 10 bar (at a total pressure of 40 bar).

The pressurized gasification of coal particles has been intensively investigated.[4,5] To the best of our knowledge, especially research on gasification kinetics of biogenic char in steam and in mixed atmospheres with H_2O partial pressures above 5 bar is scarce, while numerous studies on gasification kinetics in H_2O and H_2O-CO_2 with $p_{H_2O} \leq 5$ bar exist (for example: H_2O atmosphere, $p_{H_2O} \leq 5$ bar;[6−12] H_2O-CO_2 mixtures, $p_{H_2O} \leq 5$ bar[10−14]).

Additionally, gasification kinetics are mostly determined in a thermogravimetric analyzer (TGA).[6−9,11−13] Especially under pressurized conditions or at high reaction rates, kinetics determined in a TGA are strongly superimposed by diffusional limitations, influencing the actual reaction gas partial pressures as well as the product gas concentration in the reaction zone.[15] Since generally, the reaction rates of gasification in steam are higher than the rates of gasification in CO_2,[10−13,16−21] diffusional limitations should be considered at even lower partial pressures in the TGA.

Gasification kinetics are also investigated in fixed bed reactors under atmospheric[13,14] and elevated pressures but only up to a steam partial pressure of 5 bar.[10,16]

Consequently, there is a noticeable gap in the literature regarding kinetic data on the gasification of biogenic char in steam and steam−CO_2 mixtures at steam partial pressures above 5 bar.

To overcome this limitation in existing research, gasification kinetics of two beech wood char qualities (particle size: 50−100 μm) in steam and steam−CO_2 mixtures at steam partial pressures up to 12.5 bar conducted in a pressurized differential fixed bed reactor (dFBR)[16] are presented in this paper. In preceding publications of the research group, these beech wood char qualities were characterized and their gasification kinetics in CO_2 up to 20 bar and in H_2O up to 5 bar were determined.[10,17] In the present work, extending the experimental data to technically relevant partial pressures and atmospheres, the interaction of H_2O and CO_2 at technically relevant partial pressures is analyzed on the basis of the gasification kinetics in steam and mixtures of steam and CO_2 as well as the CO_2 kinetics.

For this purpose, experiments in the chemically controlled regime are crucial, where effective reaction rates are not dominated by mass transport rates through the boundary layer around the particle, as well as the particle's porous structure and the micro-kinetics of the reaction are measurable.[18] For the heterogeneous gasification of wood-derived char particles such as those investigated here, the chemically controlled regime is found for temperatures below 900 °C and particle diameters up to 150 μm.[15]

The micro-kinetics in a single-gas atmosphere are modeled either by a power law (PL) or a Langmuir−Hinshelwood (LH) expression. The PL approach describes a simple, empirical partial pressure dependence of the reaction rates by means of the reaction order n, for example, as shown in eq 3 in the case of steam atmosphere

$$r_{PL,H_2O} = k_{H_2O} \cdot p_{H_2O}^{n} \quad (3)$$

Especially if surface saturation occurs with increasing partial pressures, the Langmuir−Hinshelwood (LH) model can be used.[19,20] For the heterogeneous gasification reactions, a simplified LH mechanism originally proposed by Laurendau[21] is widely accepted.[10,22−24] The mechanism is based on the formation and desorption of the carbon−oxygen complexes C(O). For CO_2 gasification, k_1 and k_2 describe the dissociative adsorption of CO_2 to a free reactive carbon center C_f and the corresponding back-reaction (the desorption of CO_2). k_3 describes the desorption of the C(O) complex forming CO

$$k_1: \ C_f + CO_2 \rightarrow C(O) + CO \quad (4)$$

$$k_2: \ C(O) + CO \rightarrow C_f + CO_2 \quad (5)$$

$$k_3: \ C(O) \rightarrow CO \quad (6)$$

The reaction rate is expressed by the rate of desorption of the C(O) complex (k_3) and assuming a steady-state concentration of C(O)[10,22,23]

$$r_{CO_2} = \frac{k_1 p_{CO_2}}{1 + \frac{k_2}{k_3} p_{CO} + \frac{k_1}{k_3} p_{CO_2}} \quad (7)$$

For the differential operation of the laboratory fixed bed reactor dFBR (see Section 2), low degrees of conversion of the gas phase and therefore negligible influence of the product gas concentrations can be inferred.[16] Product gas inhibition can thus be omitted ($p_{CO} \ll p_{CO_2}$) and eq 7 is simplified to eq 8

$$r_{CO_2} = \frac{k_1 p_{CO_2}}{1 + \frac{k_1}{k_3} p_{CO_2}} \quad (8)$$

The H_2O gasification mechanism is more complex because not only carbon−oxygen complexes but also different types of carbon−hydrogen complexes exist.[21] As product gas concentrations can be considered negligible, from the mechanism consisting of seven reactions,[10] only those related to the dissociative adsorption of the H_2O molecule (k_4) and the formation and desorption of the product gas CO (k_6) are regarded here

$$k_4: \ C_f + H_2O \rightarrow C(O) + H_2 \quad (9)$$

$$k_5: \ C(O) + H_2 \rightarrow C_f + H_2O \quad (10)$$

$$k_6: \ C(O) \rightarrow CO \quad (11)$$

Analogous to eqs 7 and 8, the reaction rate in steam is formulated (eq 12) as

$$r_{H_2O} = \frac{k_4 p_{H_2O}}{1 + \frac{k_4}{k_6} p_{H_2O}} \quad (12)$$

A derivation of eqs 7, 8, and 12 can be found in Section S.1.

https://doi.org/10.1021/acs.energyfuels.5c04287
Energy Fuels XXXX, XXX, XXX−XXX

The temperature dependence of the rate constants k_i in eqs 3, 7, 8, and 12 are described by the Arrhenius equation (eq 13)

$$k = k_0 \exp\left(-\frac{E_A}{R_U T}\right) \tag{13}$$

The determination of the kinetic parameters for the LH or PL model requires gasification experiments with temperature and pressure variation. Zhao et al. varied the temperature in the range of 725−900 °C and steam partial pressures in the range of 0.1−0.7 bar in gasification experiments with corn stalk char. Saturation of the char surface for $p_{H_2O} \geq 0.5$ bar was found. Accordingly, the LH model could predict the gasification rates.[8] In contrast, Schneider et al.[10] did not observe any indication of surface saturation for two types of beech wood char in gasification experiments at temperatures of 830−870 °C and steam partial pressures up to 5 bar. The kinetics were consistently modeled with a power law approach.[10] Comparison of the results by Zhao et al. and Schneider et al. clearly shows that saturation of the biomass char surface can occur at subatmospheric steam partial pressures or remain irrelevant even at higher steam partial pressures.

1.1. Interaction of H_2O and CO_2 on the Char Surface. Different types of interactions between mixtures of H_2O and CO_2 and the reactive carbon surface during gasification have been reported in the literature. Comprehensive literature reviews or summaries can for example be found in refs 11,19,25. The interaction is mostly categorized into four cases, namely, additive, competitive, partially additive (partially competitive), and synergistic.

Key factors for the distinction between the first three cases are the partial pressures of the reactant gases steam and CO_2 and the amount and nature of the reactive sites (same or distinct reactive sites for H_2O and CO_2) and their reactivity.

If the char surface presents distinct reactive sites for the heterogeneous water−gas reaction and the Boudouard reaction, then both reactions take place independent of each other. The reaction rate of the mixed atmosphere can be expressed as the sum of the reaction rates in single-gas atmospheres (eq 14). The additive mechanism is therefore also known as a separate active sites mechanism

$$r_{add}(T, p_{H_2O}, p_{CO_2}) = r_{H_2O}(T, p_{H_2O}) + r_{CO_2}(T, p_{CO_2}) \tag{14}$$

If the reactive char surface presents the same reaction partners to steam and CO_2, then both adsorb to and react with the same reactive sites. Practically, the reaction rate of the mixed atmosphere can be expressed as the sum of the reaction rates in single-gas atmospheres as long as the reactive surface is not saturated yet. On the saturated reactive surface, H_2O and CO_2 compete for the same sites.[19,25,26]

A common expression to describe the competitive mechanism is based on the LH model.[10,22] In eq 15, k_1 and k_3 are derived for the LH model describing CO_2 gasification, while k_4 and k_6 are obtained for H_2O gasification (see eqs 8 and 12)

$$r_{comp} = \frac{k_1 p_{CO_2} + k_4 p_{H_2O}}{1 + \frac{k_1}{k_3} p_{CO_2} + \frac{k_4}{k_6} p_{H_2O}} \tag{15}$$

The transitions from an apparently additive behavior to a competitive behavior have been observed at atmospheric total pressure[27−29] as well as higher total pressures[5,30] for coal chars, indicating that no definitive statement could be made. In the publications dealing with gasification of biogenic char in H_2O−CO_2 mixtures at atmospheric total pressure, only additive behavior was found.[11,14] Since the mode of interaction between H_2O and CO_2 on the char surface has a significant impact on the reaction rate, it is essential for research on EFG to investigate their interaction at technically relevant partial pressures.

The partially shared reactive site mechanism assumes three different types of reactive sites on the char surface with different adsorption and reaction kinetics. The surface presents reactive sites that can exclusively react with H_2O or CO_2 as well as sites that are susceptible to both molecules. Different models for this mechanism have been presented in the literature.[26,31,32] For example, in Umemoto's approach, the ratios of reactive sites uniquely accessible for CO_2 respectively steam to shared reactive sites, and the ratios between unoccupied reactive CO_2 sites to H_2O sites are introduced as new fitting parameters. The fitting parameters are difficult to be verified experimentally. Therefore, the partially shared reactive sites approach is not further considered.

The synergistic mechanism results in reaction rates in the mixture that are larger than the sum of the reaction rates in single-gas atmospheres. As will be concretized in the following, synergy is likely to result from beneficial effects of catalytic activity and/or pore evolution during gasification in H_2O−CO_2 mixtures and is not directly attributed to the nature and saturation of the reactive surface.[25,26,33−35] For this reason, synergistic reaction mechanisms should not occur separately but should be superimposed on additive or competitive mechanisms. It is conceivable that this effect belongs to a narrow range of the H_2O and CO_2 partial pressures, as beneficial morphological developments depend on the reaction gas partial pressures and are antagonized by deactivation of catalytically active species. Additionally, when H_2O and CO_2 compete for the same reactive sites, synergy is also likely to be ruled out. This and the fact that experimental matrices are often small might be the reasons why it is rarely reported that the reaction rate in the mixed gasification atmosphere is significantly larger than the sum of the reaction rates in single-gas atmospheres.

1.2. Influence of Chemical and Structural Properties of the Char. The chemical properties of the char include the amount of reactive carbon sites (or the reactive surface area) and the type and dispersion of active minerals with catalytic or inhibitory effect and therefore affect the rate of the micro-kinetics and the interaction of H_2O and CO_2 on the char surface.[36,37]

The amount of reactive carbon sites on the carbon surface depends on the structure of the carbon matrix, especially on the degree of graphitization.[17,24,38,39] The graphitization degree increases with severity of heat treatment (e.g., temperature and residence time), and the reaction rate decreases as the graphitization degree increases.[17,40,41] In the scientific literature discussing the interaction of H_2O and CO_2, the role of graphitization has rarely been considered. In the work at hand, explanatory approaches incorporating graphitization will be included.

Especially the alkaline and alkaline-earth metals potassium, sodium, calcium, and magnesium are known to catalyze both heterogeneous gasification reactions.[17,37,42−44] Calcium, followed by silicon and potassium, is one of the most abundant

https://doi.org/10.1021/acs.energyfuels.5c04287
Energy Fuels XXXX, XXX, XXX−XXX

inorganic elements in wood.[45] Potassium is a stronger catalyst in both gasification reactions.[13,37,44] Unlike calcium, potassium devolatilizes from the char surface at 800 °C, and only intercalated or organically bound potassium remains more stably.[13,46] The interaction of potassium with silicon and phosphorus can cause inhibition of potassium catalysis of the heterogeneous water−gas reaction, while in the case of the Boudouard reaction, mainly silicon reveals inhibitory effects on potassium catalysis. The extent of inhibition is often estimated by the ratio of potassium to silicon (Boudouard reaction) or potassium to silicon and phosphorus (heterogeneous water−gas reaction).[42,43,47]

The effect of catalyst dispersion on the char surface on the catalytic activity was also investigated for the Boudouard reaction with the clear result that a fine catalyst dispersion has a positive effect.[17,48,49]

Different groups investigated the interaction between calcium as a catalyst and the pore structure during gasification by means of various char types such as bituminous and subbituminous coal char,[33,35] lignite char,[50] calcium-loaded coal char,[33,51] beech wood char,[12] or rice husks and sunflower seed shells.[9] Gasification experiments were conducted at 800−900 °C and at steam and CO_2 contents between 20 and 100% at atmospheric pressure, respectively. Scanning electron microscopy (SEM) and physisorption analyses of the partially gasified chars revealed that during Ca-catalyzed steam gasification (impregnated or naturally present calcium), a so-called "channeling mode" led to stronger evolution and enlargement of pores in the carbon matrix than during Ca-catalyzed CO_2 gasification.[51] Different authors report a honeycomb pore structure when CaO particles on the char surfaces entrain into the carbon matrix with proceeding carbon conversion in H_2O atmosphere.[35,51] Steam gasification thereby led to a strong increase in specific surface area up to 60−75% conversion.[9,30,33,50,51] While during gasification with steam, new micropores were created and existing pores enlarged, CO_2 gasification only led to an increase in microporosity.[33] Supported by the observation that pore development was weaker and the char surface looked pitted in the case of Ca-catalyzed CO_2 gasification, Yu et al. and Guizani et al. assigned a more surface-concentrated reaction mode to the catalyzed C−CO_2 reaction ("surface recession mode").[12,51]

Moreover, the observations can be ascribed to a higher self-diffusion coefficient and better molecular diffusion of H_2O compared to CO_2[25,35] and better access to micropores of steam.[52]

Morphological analysis of partially gasified chars from the mixed gasification atmosphere showed that steam predominated the morphological evolution of the char during gasification in mixtures of steam and CO_2.[12,33,35,50,53] The formation and enlargement of pores due to Ca-catalyzed C−H_2O reaction could promote CO_2 diffusion into the char particle volume and enlarge the reactive surface area, thus enhancing the C−CO_2 reaction.[12,26,33,35,50] Wedler et al. developed a pore-structure-dependent kinetic adsorption model for CO_2, clearly showing that the mass transport through macro- and mesopores and the adsorption on their surface is faster than for micropores.[54] This supports the assumption that especially pore enlargement due to steam gasification enhances CO_2 diffusion and reaction. Moreover, Gao et al. suggest that the presence of steam in a mixed gasification atmosphere reduces sintering of calcium particles, also maintaining the catalysis of the C−CO_2 reaction at a higher level than in the presence of solely CO_2.[33] These are possible explanations for positive enhancement between CO_2 and steam during mixed gasification, thus the synergy.

2. MATERIALS AND METHODS

2.1. Beech Wood Char Qualities Investigated. As mentioned briefly in the beginning of this paper, the char samples used for the reaction kinetic experiments reported here were already investigated in previous works of the research group.[10,17] The following section summarizes the previous works[10,17] in order to provide necessary information on the char qualities.

As described in the Introduction, primary char particles from the fast pyrolysis preprocessing step fed to the EFG reactor undergo secondary pyrolysis at high temperatures and high heating rates. To receive secondary char particles that underwent a comparable time−temperature history as the char particles in the EFG reactor and that were produced at defined conditions, primary beech wood char particles produced under mild conditions (500−600 °C) were subjected to a secondary pyrolysis in a laboratory-scale drop-tube reactor.[17] The primary beech wood char was pyrolyzed at 1400 °C (P1400) and 1600 °C (P1600) and with a residence time in the isothermal zone of the drop-tube reactor of 200 ms.[17] Thereby, also the influence of the secondary pyrolysis in the EFG reactor on the char properties and char reactivity was assessed.[17]

The particle size fraction of 50−100 μm was chosen based on its general significance for the gasification process (particles up to 500 μm,[41] usually smaller[55,56]) as well as its use in prior studies on EFG conducted at KIT.[10,15,17,24,55]

Graphitization of the resulting secondary chars was analyzed with X-ray diffraction and Raman spectroscopy.[17] As expected, the degree of graphitization was higher for P1600, which was especially seen by means of the radial expansion of the graphene layers (P1400: L_a = 2.9 10^{-9} m vs P1600: L_a = 3.2·10^{-9} m).[17] Since this study primarily focuses on the comparison between the two char types, graphitization will hereafter be referred to simply as "higher" (P1600) and "lower" (P1400). The dispersion of calcium was determined by chemisorption and transmission electron microscopy coupled with energy-dispersive X-ray spectroscopy.[17] Interestingly, CaO particles were more finely dispersed on the surface of P1600, which was traced back to their better mobility at higher pyrolysis temperatures. The micropore surface area was larger for P1400.[17] A summary is given in Table 1.

Table 1. Beech Wood Char Qualities Investigated and Relevant Properties[10,17]

	P1400	P1600
pyrolysis temperature (drop-tube reactor)	1400 °C	1600 °C
Proximate Analysis/wt %, ad		
moisture	0.2	0.0
ash content	1.9	1.6
volatiles	2.5	1.3
fixed carbon	95.4	97.1
Ultimate Analysis/wt %, daf		
C	97.2	99.0
H	0.2	0.2
N	0.7	0.5
O (by difference)	1.9	0.3
Selected Ash Components/wt % ash		
Ca	35.3	39.1
K	5.48	5.05
Si	2.51	2.45
P	1.73	1.52
micropore surface area/m^2 g^{-1}	660	126.4
CaO dispersion	coarse	fine
graphitization	lower	higher

https://doi.org/10.1021/acs.energyfuels.5c04287
Energy Fuels XXXX, XXX, XXX−XXX

From the gasification experiments in CO_2 partial pressures up to 20 bar, it turned out that char type P1600 showed higher reactivity in CO_2 than char type P1400. The authors assigned it to the high dispersion of calcium on the surface of P1600. For char type P1600, experiments indicated saturation at a CO_2 partial pressure above 10 bar. Accordingly, the LH model best described the reaction kinetics of P1600. On the contrary, the CO_2 gasification kinetics of char type P1400 were better described by the PL model.[10]

The reaction rate in a mixed atmosphere with $p_{CO_2} \leq 5$ bar and $p_{H_2O} \leq 5$ bar could be described by an additive approach in the whole partial pressure range for P1400 and until H_2O and CO_2 partial pressures of 2 bar, respectively, for P1600.[10]

2.2. Pressurized Differential Fixed Bed Reactor (dFBR). The dFBR is designed to investigate the micro-kinetics of the gasification reactions at a maximum total pressure of 20 bar with steam partial pressures up to 12.5 bar and CO_2 partial pressures up to 20 bar. The dFBR is operated differentially, meaning that the concentration gradients of the educt and product gases in the sample bed are small enough to neglect their influence on the reaction rate. This is achieved by small sample masses. In refs 16, a criterion was developed to verify the differential operation.

A detailed description of the dFBR, the experimental procedure, and the data evaluation has been recently published.[16] A flow scheme of the dFBR can be found in Supporting Information S2. In the following, a brief description of the main components of the laboratory plant, the experiments, and the data evaluation is given.

The main part of the reactor is the electrically heated reactor tube. The applicable gases H_2O, CO_2, and argon vertically flow through a differential bed of char particles on a quartz glass sample holder mounted in the reactor. The reaction temperature is monitored with a type K thermocouple inserted close to the sample bed.

A bypass strand and two 4-port 2-position valves upstream and downstream the reactor allow preparation of the reaction gas atmosphere while leading it through the bypass strand. For the reaction gas atmosphere, steam is generated and mixed with argon and eventually CO_2 in a controlled evaporation and mixing unit operated at 200 °C. By switching the 4-port 2-position valve upstream the reactor, the reaction gas atmosphere is led to the reactor and the char sample. The 4-port 2-position valve downstream the reactor serves to lead the product gases to the gas analyzers or the vent.

Steam is condensed and discharged in steam traps after the reactor and in the bypass strand. Pressure regulators are mounted downstream of each steam trap. The analysis of the dry and atmospheric product gases is done by an infrared photometer and a micro-gas chromatograph or a mass spectrometer. Due to the volume changing gasification reactions and the condensation of steam, a defined reference flow of nitrogen is added just before the gas analyzers to determine the actual volume and molar flow rates of the product gases.

All steam-carrying pipes can be electrically heated.[16]

2.3. Experimental Procedure. Prior to each experiment, the reactor was heated to the desired reaction temperature of 810–870 °C and the electrical heatings of all steam-carrying pipes were set to 200–250 °C. During this procedure, the reactor and all pipes were flushed with argon. Subsequently, the sample batch of up to 54 mg was dosed into the hot reactor and on the sample bed with a mobile, argon-flushed dosing unit. According to previous investigations, 10–54 mg is a suitable sample mass range for differential operation.[16]

The reactor was then pressurized in argon. Meanwhile, the reaction gas atmosphere consisting of H_2O, eventually CO_2 and argon, was adjusted in the bypass strand at the desired pressure. Volume flows were adjusted to achieve a uniform flow velocity of 10.5 cm/s in the reactor tube for all reaction temperatures and pressures. By switching from the bypass strand to the reactor, the reaction gases then flew through the reactor strand, and carbon conversion started. As mentioned above, the product gases are analyzed with an infrared photometer and a micro-gas chromatograph or a mass spectrometer. The experiment was terminated when the product gas concentrations were below 5–10 ppm. Each experiment was repeated 2–3 times.[16]

A first set of gasification experiments was conducted in mixtures of steam and argon to determine the reaction kinetics of the heterogeneous water–gas reaction. Table 2 summarizes the experiments conducted in a H_2O and argon atmosphere.

Table 2. Experimental Parameters for Steam Gasification Experiments with Char Types P1400 and P1600

$T_{reaction}$ / °C	p_{tot} / bar	p_{H_2O} / bar
810	5	2
810, 830, 850, 870	10	5
810, 830, 850, 870	20	7.5, 10, 12.5

In a second set of experiments with mixtures of H_2O and CO_2, H_2O partial pressures of 2–9 bar and CO_2 partial pressures of 9–17.5 bar at temperatures of 810–850 °C were set. Table 3 gives an overview of the experiments in a mixed atmosphere. The experiments with increasing H_2O partial pressure between 4.5 and 9 bar at constant CO_2 partial pressure of 9 bar were conducted to observe the gasification behavior at increasing H_2O partial pressure in the mixture with a technically relevant partial pressure of CO_2. The experiments at high CO_2 partial pressures of 14.5 and 17.5 bar were conducted to clarify the influence of increasing CO_2 partial pressures.

Table 3. Experimental Parameters for Mixed Gasification Experiments with Char Types P1400 and P1600

$T_{reaction}$ / °C	p_{tot} / bar	p_{H_2O} / bar	p_{CO_2} / bar
810, 830, 850	20	4.5	9
		4.5	14.5
		2	17.5
		7.5	9
		9	9

2.4. Data Evaluation: Mass Balance and Carbon Conversion. The molar flow rates of the product gases are determined by referring the measured concentrations to the concentration of the reference gas nitrogen (eq 16)

$$\dot{n}_i = \frac{\dot{V}_{N_2}}{y_{N_2}} \cdot \frac{y_i}{V_{molar}} \tag{16}$$

The converted mass of carbon $m_{C,conv}$ at time t_i is determined by eq 17 below

$$m_{C,conv}(t_i) = m_{C,conv}(t_{i-1}) + \tilde{M}_C \cdot \frac{1}{2}(\dot{n}_{CO}(t_i) + \dot{n}_{H_2}(t_i)) \cdot (t_i - t_{i-1}) \tag{17}$$

The carbon conversion $X_{C,gasif}(t_i)$ in reference to the total mass of gasified carbon $m_{C,gasif}$ (eq 18) is then calculated by eq 19

$$m_{C,gasif} = m_{C,conv}(t_{end}) \tag{18}$$

$$X_{C,gasif}(t_i) = \frac{m_{C,conv}(t_i)}{m_{C,gasif}} \tag{19}$$

The carbon conversion rate $dX_{C,gasif}/dt$ is determined accordingly (eq 20)

$$\frac{dX_{C,gasif}}{dt} = \frac{\tilde{M}_C \cdot \frac{1}{2}(\dot{n}_{CO}(t_i) + \dot{n}_{H_2}(t_i))}{m_{C,gasif}} \tag{20}$$

The reactivity R_{UCM} was determined by adjusting the Uniform Conversion Model (UCM) (eq 21) to the experimentally derived conversion $X_{C,gasif}$ for a conversion range of $0 \leq X_{C,gasif} \leq 0.8$ with a least-squares approach and taking into account the system response behavior of the dFBR. The system response behavior was intensively studied in refs 16 with the clear result that integration of the response

https://doi.org/10.1021/acs.energyfuels.5c04287
Energy Fuels XXXX, XXX, XXX–XXX

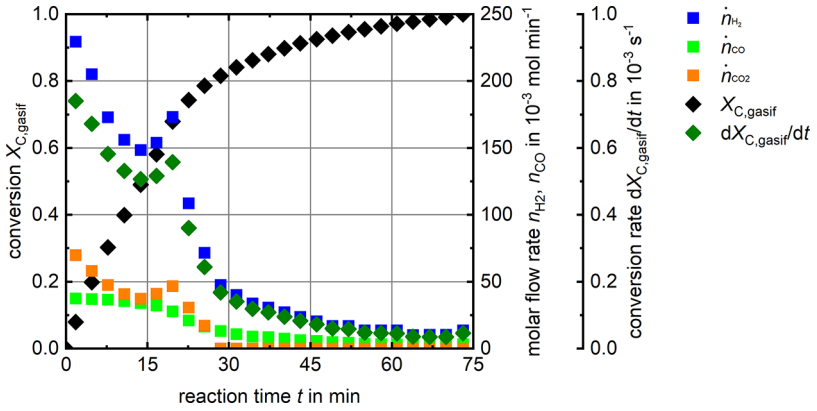

Figure 1. Conversion, conversion rate, and molar flow of product gases of char type P1400 (experiment at $T_{reaction}$ = 810 °C, p_{tot} = 20 bar, p_{H_2O} = 7.5 bar).

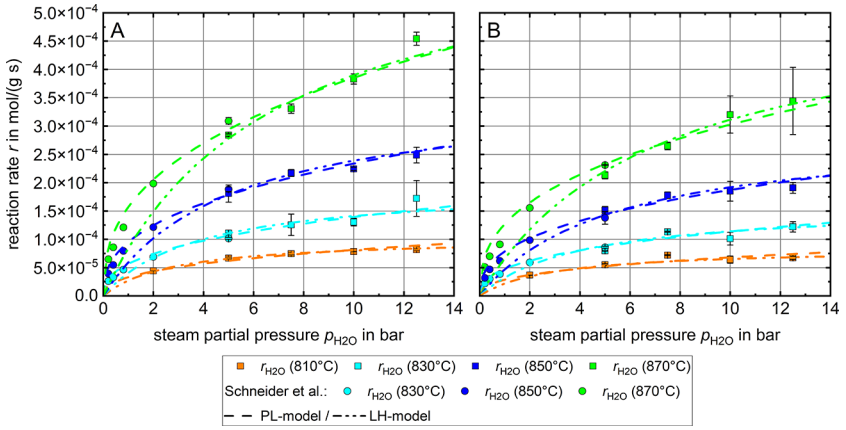

Figure 2. Influence of H_2O partial pressure on the reaction rate of the heterogeneous water−gas reaction of P1400 (A) and P1600 (B) (810 °C ≤ $T_{reaction}$ ≤ 870 °C, 2 bar ≤ p_{H_2O} ≤ 12.5 bar) and PL and LH model.

behavior in the data evaluation routine is crucial especially for fast kinetics at high H_2O partial pressures

$$X_C(t) = 1 - \exp(-R_{UCM} \cdot t) \tag{21}$$

The reaction rate r was then determined following eq 22[16]

$$r = \frac{R_{UCM}}{\tilde{M}_C} \tag{22}$$

The temperature and partial pressure dependence of the reaction rates was modeled with the Arrhenius approach in combination with the PL and LH model. To assess the interaction of H_2O and CO_2 during mixed gasification, the additive expression (eq 14) and the competitive expression (eq 15) were determined based on the H_2O kinetics derived in this work and the CO_2 kinetics by refs 10.[10]

3. RESULTS AND DISCUSSION

3.1. Evolution of the Conversion Rate during Gasification. Figure 1 exemplarily depicts the molar flow rates of H_2, CO, and CO_2, the carbon conversion $X_{C,gasif}$ and the conversion rate $dX_{C,gasif}/dt$ from a gasification experiment with char type P1400 at p_{H_2O} = 7.5 bar, p_{tot} = 20 bar, and $T_{reaction}$ = 810 °C. The product gas contains CO_2 although it is not a product of the heterogeneous water−gas reaction. This can be explained by the reverse water−gas shift reaction from H_2O and CO.[16]

In the experiment shown in Figure 1, the product gas molar flows of CO, H_2, and CO_2 first decrease with increasing carbon conversion, then a shoulder or local maximum between 0.5 ≤ $X_{C,gasif}$ ≤ 0.8 can be observed. With further increasing carbon conversion, the molar flow rates approach 0 mol/min. Following eq 20, the time course of the conversion rate is similar to the time course of the product gas molar flow rates, and it also shows a maximum between 0.5 ≤ $X_{C,gasif}$ ≤ 0.8. This observation (shoulder or local maximum) was made at $X_{C,gasif}$ ≥ 0.5 for all experiments in H_2O and in H_2O−CO_2 mixtures for both char types. The shoulder or maximum was more pronounced for char type P1400. For more examples, see Supporting Information S3.

Schneider et al. observed a similar behavior during their experiments at lower H_2O partial pressures for conversion degrees of 70−80% and assigned it to the fragmentation of the char particles, leading to a sudden increase in the reactive surface area (at high conversion levels, the particles become very fragile and may suddenly disintegrate into many small fragments, leading to a significant and abrupt increase in the external surface area).[10] Besides the explanation in refs 10, other approaches to explain this remarkable evolution are conceivable. One first possible explanation could be the strong increase in surface area up to 60−75% conversion due to calcium-catalyzed steam gasification, followed by a collapse of the pore structure as reported in the literature.[9,25,30,33,50,51] Due to the collapse of the pore structure, a sudden reduction of the surface area leads to a strong decrease in the conversion rate.[57]

https://doi.org/10.1021/acs.energyfuels.5c04287
Energy Fuels XXXX, XXX, XXX−XXX

Following Dupont et al.,[43] potassium catalysis of the heterogeneous water−gas reaction leads to a shoulder or maximum of the conversion rate at $X_{C,gasif} \geq 0.5$ if the ratio of mass fractions of potassium, silicon, and phosphorus K/(Si + P) is equal to or higher than one. The K/(Si + P) ratios of the two beech wood char qualities are 1.29 (P1400) respectively 1.27 (P1600),[17] indicating that the evolution of product gas concentrations and conversion rate can be assigned to potassium catalysis of the C−H_2O reaction.[43] Unlike the dispersion of calcium, the dispersion of potassium found by transmission electron microscopy is fine for both char types and the potassium content is in the same order of magnitude as well, thus comparable catalytic activity of potassium can be postulated for both.[17]

The UCM used for kinetic analysis describes a steady decrease in the conversion rate with increasing conversion. As the model cannot follow the observed increase of the conversion rate at $X_{C,gasif} \geq 0.5$, the applicability of the UCM was assessed with the result that for large fitting conversion ranges of $0 \leq X_{C,gasif} \leq 0.8$, the deviation from model behavior has only minor impact on the derived reaction rate (see Supporting Information S3).

3.2. Gasification at Elevated Steam Partial Pressures. For the sake of completeness, the results of refs 10 are also depicted in this work and marked in the following diagrams. Some selected experiments of refs 10 were repeated in order to verify consistency between the data of Schneider et al. and the data reported in this work (see Supporting Information S4).

Figure 2 shows the reaction rates of the heterogeneous water−gas reaction determined for 810−870 °C and H_2O partial pressures between 2 and 12.5 bar. The experimentally determined reaction rates are given in Supporting Information S5. The reaction rates for 810 °C and reaction rates for $p_{H_2O} \geq 5$ bar for 830−870 °C in Figure 2 A (reaction rates of P1400, squares) have already been published in a previous work focusing on the differential operation and on the system response behavior of the dFBR.[16]

For both char types, an increase in p_{H_2O} comes along with a significant increase in the reaction rate, indicating that the reactive surface area is not saturated. The reaction rates in H_2O of char type P1400 are higher than those of char type P1600, suggesting that the lower degree of graphitization and the higher micropore surface area of char type P1400 play a more important role for the H_2O gasification reaction than the higher dispersion of calcium of P1600. The carbon matrix of P1400 is less graphitized, i.e., less ordered and contains more carbon edges or dislocations.[21] Therefore, the surface of P1400 should present more reactive sites than the surface of P1600.

Additionally, as presented in the introductory part, especially H_2O molecules can access micropores. Consequently, both the higher micropore surface area and the higher number of reactive sites per char surface of P1400 are most likely responsible for the higher conversion rate and mass-specific reaction rate in the H_2O atmosphere.

Compared to the reaction rates in CO_2,[10] the reaction rate for H_2O is higher than for CO_2, as widely reported in the literature (e.g., see refs 10−13,34).

The parameters of the PL model and the LH model were fitted to the experimental data of this work (reaction rates for 810 °C and reaction rates for $p_{H_2O} \geq 5$ bar for 830−870 °C). Both models can describe the reaction kinetics for higher H_2O partial pressures above 5 bar. Especially, the PL model also represents the data at low H_2O partial pressures. Tables 4 and 5 summarize the modeling results.

Table 4. Kinetic Parameters for the Heterogeneous Water−Gas Reactions of P1400 and P1600 Using the PL Model

		P1400	P1600
k_{0,H_2O}	mol (g·s·bar$^{n_{H2O}}$)$^{-1}$	$2.4 \cdot 10^8$	$6.6 \cdot 10^7$
E_{A,H_2O}	kJ mol^{-1}	266.7	256.3
n_{H_2O}		0.39	0.38

Table 5. Kinetic Parameters for the Heterogeneous Water−Gas Reactions of P1400 and P1600 Using the LH Model

		P1400	P1600
k_{04,H_2O}	mol (g·s·bar)$^{-1}$	$3.2 \cdot 10^3$	$2.0 \cdot 10^3$
$E_{A,4,H_2O}$	kJ mol^{-1}	164.7	162.6
k_{06,H_2O}	mol (g·s)$^{-1}$	$2.2 \cdot 10^{11}$	$1.5 \cdot 10^{11}$
$E_{A,6,H_2O}$	kJ mol^{-1}	318.1	316.0

The activation energies of P1400 and P1600 differ by less than 5% (for the PL model as well as the LH model). This indicates that the reactive sites for the C−H_2O reaction on the surface of both char types are similar. On the contrary, the preexponential factors of the kinetics belonging to P1400 are considerably higher than those belonging to P1600. This can be explained by the aforementioned higher number of reactive sites per surface area and the larger micropore surface area of char type P1400, resulting in a higher total number of reactive sites and therefore higher preexponential factors and a higher mass-specific reaction rate. In turn, the calcium dispersion seems to be less important for the gasification reaction with steam.

3.3. Gasification in Steam−CO_2 Mixtures at Elevated Pressures. Table 6 summarizes the investigated combinations of H_2O and CO_2 partial pressures, as introduced in Section 2. For ease of reference in Figure 7, identifiers (A−E) are assigned in Table 6 and used in the next section.

Table 6. Partial Pressure Combinations of H_2O and CO_2 Investigated

identifier	A	B	C	D	E
p_{H_2O}/bar	4.5	7.5	9	4.5	2
p_{CO_2}/bar	9	9	9	14.5	17.5

Figures 3−6 present the experimental reaction rates (triangles, r_{exp}) as well as the reaction rates calculated for the additive (circles, r_{add}) and competitive mechanisms (squares, r_{comp}). The reaction rates of additive model r_{add} (eq 14) of P1400 are calculated with the PL model parameters for H_2O and CO_2 gasification. For P1600, r_{add} is modeled analogously but with the LH parameters of CO_2, as the LH model provided the best fit to the experimental data.[10] The reaction rates of competitive model r_{comp} (eq 15) are calculated with the LH model parameters for H_2O and CO_2 gasification. PL model parameters for H_2O are listed in Table 4, and for CO_2 they are listed in Table 7. The LH model parameters for char types P1400 and P1600 are provided in Tables 8 and 9, respectively.

https://doi.org/10.1021/acs.energyfuels.5c04287
Energy Fuels XXXX, XXX, XXX−XXX

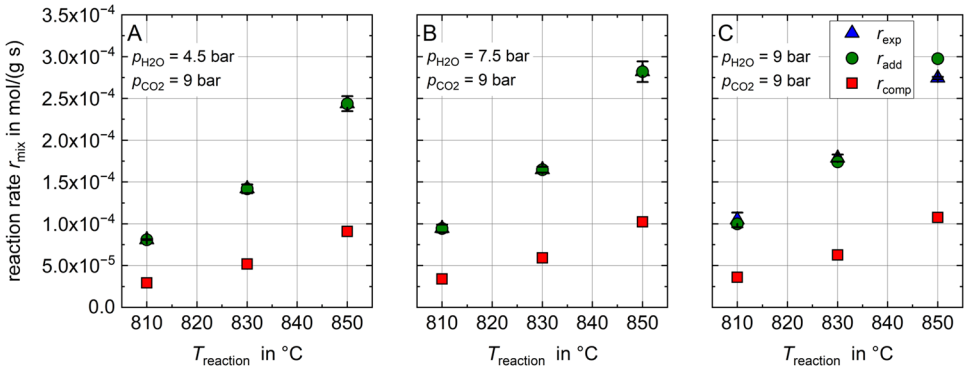

Figure 3. P1400: experimental reaction rates of mixed gasification r_{exp} with error bars for increasing H_2O partial pressures of 4.5 bar (A), 7.5 bar (B), and 9 bar (C) at a CO_2 partial pressure of 9 bar and at 810−850 °C versus additive and competitive models (r_{add} and r_{comp}).

Table 7. Kinetic Parameters for the Boudouard Reaction of P1400 and P1600 Using the PL Model Taken from Refs 10

		P1400	P1600
k_{0,CO_2}	mol (g·s·bar$^{n_{CO2}}$)$^{-1}$	$1.016 \cdot 10^{10}$	$5.68 \cdot 10^{9}$
E_{A,CO_2}	kJ mol^{-1}	308.7	300.7
n_{CO_2}		0.21	0.19

If r_{exp} differs by less than 10% from r_{add} or r_{comp}, then the approach is considered adequate. The values of r_{exp}, r_{add}, and r_{comp} and the deviations are given in Section S.5.

Figure 3 A−C shows the reaction rates for char type P1400 with increasing H_2O partial pressures of p_{H_2O} = 4.5 bar, p_{H_2O} = 7.5 bar and p_{H_2O} = 9 bar at a constant CO_2 partial pressure of p_{CO_2} = 9 bar. The reaction rates r_{exp} deviate by less than 10% from r_{add}, indicating an additive behavior. With refs 10 that assigned additive behavior to the reaction rates in the mixture up to p_{CO_2} = 5 bar and p_{H_2O} = 5 bar, it can be stated that the additive mechanism holds true for partial pressure combinations up to p_{H_2O} = 9 bar and p_{CO_2} = 9 bar. From a mechanistic view, up to p_{H_2O} = 9 bar and p_{CO_2} = 9 bar, enough reactive surface area is available for the H_2O and CO_2 molecules because the degree of graphitization is sufficiently low.

Figure 4 A,B presents the reaction rates with CO_2 partial pressures of p_{CO_2} = 14.5 bar and p_{CO_2} = 17.5 bar for char type P1400. In this higher CO_2 partial pressure range, the reaction rates r_{exp} lie between those predicted by the additive and competitive model formulations. The experimental reaction rates are overestimated by r_{add} by 20% on average. The partial pressure combinations in Figure 4 are therefore assigned to the transition between the additive and competitive behavior. This indicates that at a CO_2 partial pressure p_{CO_2} > 9 bar, the reactive surface area cannot provide sufficient unoccupied reactive sites anymore.

For char type P1600, the additive behavior was assigned to $p_{CO_2} \leq 2$ bar and $p_{H_2O} \leq 2$ bar with a transition to competitive behavior for higher H_2O and CO_2 partial pressures because the experimental reaction rates in the mixture were found between the reaction rates from the additive and competitive models.[10]

In line with these previous observations, the reaction rates at p_{CO_2} = 14.5 bar and p_{H_2O} = 4.5 bar (Figure 5 A) are situated between the additive and competitive model predictions, with the additive model showing an average overestimation of 51%. At p_{CO_2} = 17.5 bar and p_{H_2O} = 2 bar (Figure 5 B), the reaction rates are overestimated by the additive approach by 18% on average. Altogether, a transition to competitive kinetics is confirmed as H_2O and CO_2 partial pressures increase. In the case of char type P1600, the transition can be observed at lower partial pressures in H_2O and CO_2 than in the case of char type P1400 (additive behavior only for $p_{CO_2} \leq 2$ bar and $p_{H_2O} \leq 2$ bar). This is traced back to the lower number of reactive sites per surface area due to stronger graphitization.

Figure 6 A−C shows the reaction rates of char type P1600 with increasing H_2O partial pressure (p_{H_2O} = 4.5 bar, p_{H_2O} = 7.5 bar and p_{H_2O} = 9 bar) at constant CO_2 partial pressure (p_{CO_2} = 9 bar). Comparison of A, B, and C reveals that r_{exp} increases with increasing H_2O partial pressure from 4.5 bar (A) to 7.5 bar (B) and decreases from 7.5 to 9 bar (C). Interestingly, in Figure 6 A,B at 810 and 830 °C, the reaction rates r_{exp} are higher than r_{add} (17% (A) and 19% (B) underestimation by r_{add} on average). At 850 °C in Figure 6 A,B, reaction rates r_{exp} are also underestimated by the additive mechanism but to less than 10%. This indicates synergistic behavior. The observed synergy may be explained by the beneficial effect of steam at higher partial pressures ($p_{H_2O} \geq 4.5$ bar) counteracting the sintering and agglomeration of the small calcium nanoparticles on the char surface of P1600, as also observed by Gao et al.[33] Thereby, steam

Table 8. LH Parameters for Char Type P1400

P1400	LH parameters for CO_2[10]		LH parameters for H_2O	
$T_{reaction}$	k_1	k_3	k_4	k_6
°C	10^{-5} mol (g·s·bar)$^{-1}$	10^{-5} mol (g·s)$^{-1}$	10^{-5} mol (g·s·bar)$^{-1}$	10^{-4} mol (g·s)$^{-1}$
810	3.36	2.26	3.70	1.02
830	5.86	4.24	5.16	1.94
850	10.0	7.80	7.10	3.60

https://doi.org/10.1021/acs.energyfuels.5c04287
Energy Fuels XXXX, XXX, XXX−XXX

Table 9. LH Parameters for Char Type P1600

P1600	LH parameters for CO_2[10]		LH parameters for H_2O	
$T_{reaction}$	k_1	k_3	k_4	k_6
°C	10^{-5} mol (g·s·bar)$^{-1}$	10^{-5} mol (g·s)$^{-1}$	10^{-5} mol (g·s·bar)$^{-1}$	10^{-4} mol (g·s)$^{-1}$
810	5.01	2.94	2.93	0.84
830	8.13	5.48	4.06	1.59
850	13.0	10.0	5.57	2.93

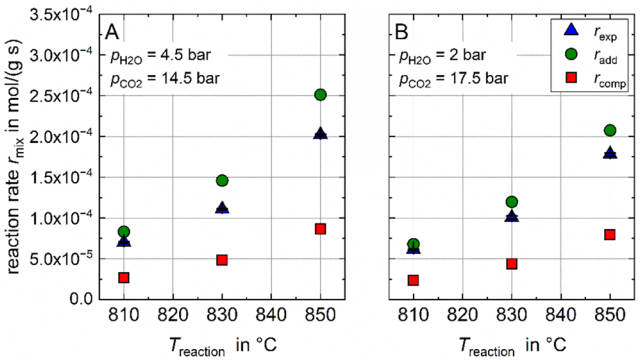

Figure 4. P1400: experimental reaction rates of mixed gasification r_{exp} with error bars for increasing CO_2 partial pressures of 14.5 bar (A) and 17.5 bar (B) at H_2O partial pressures of 4.5 and 2 bar and at 810−850 °C versus additive and competitive models (r_{add} and r_{comp}).

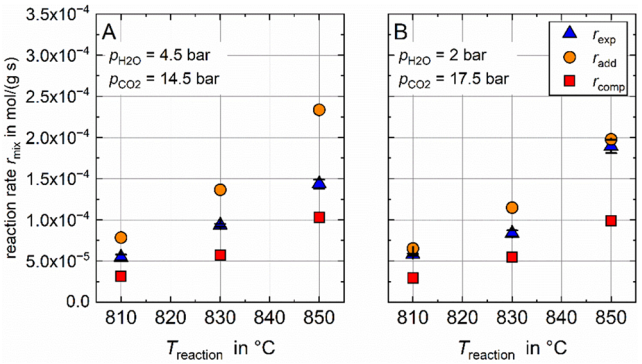

Figure 5. P1600: experimental reaction rates of mixed gasification r_{exp} with error bars for increasing CO_2 partial pressures of 14.5 bar (A) and 17.5 bar (B) at H_2O partial pressures of 4.5 and 2 bar and at 810−850 °C versus additive and competitive models (r_{add} and r_{comp}).

maintains the fine calcium dispersion and, therefore, also the calcium catalysis of the Boudouard reaction at a high level.

Comparison of r_{exp} to r_{add} and r_{comp} in Figure 6 C indicates that at steam partial pressures of p_{H_2O} = 9 bar, the interaction of H_2O and CO_2 shifts toward competitive behavior again. Hence, it is reasoned that the synergistic behavior is limited to the range of partial pressure combinations around p_{CO_2} = 9 bar and 4.5 bar ≤ p_{H_2O} ≤ 7.5 bar.

Figure 7 shows the experimentally derived reaction rates of mixed gasification at 830 °C in a heat map. The heat map is used to transfer the findings of the gasification experiments in a mixed atmosphere to EFG systems with total pressures of 40 bar.

For char type P1400, the reaction rate in steam on the abscissa of Figure 7 (p_{CO_2} = 0 bar) and the reaction rate in CO_2 on the ordinate (p_{H_2O} = 0 bar) are calculated with the PL model parameters (Tables 4 and 7). For char type P1600, H_2O kinetics for the abscissa are determined analogously (Table 4), but the CO_2 kinetics are calculated with the LH approach (Table 9).[10] Black symbols represent experimental data in mixed atmosphere of this work, gray symbols refer to experimental results in mixed atmosphere by refs 10. Dots indicate additive behavior in the respective experiment, circles indicate competitive behavior, and dots with crosses denote synergistic behavior. Linear interpolation is applied between experimental data points to generate the color map. Since the data points are unevenly spaced, the reaction rate behavior between them cannot be assumed to represent accurate values.

The approximate partial pressures of technical gasifiers are indicated in red in Figure 7.

For char type P1400, having weaker graphitization (corresponding to more reactive sites per surface area), the additive behavior is considered valid up to p_{CO_2} = 9 bar in the kinetically controlled regime. So for a technical system with p_{CO_2} ≈ 10 bar and p_{H_2O} ≈ 10 bar, the additive model gives a good approximation of the gasification rate for such chars.

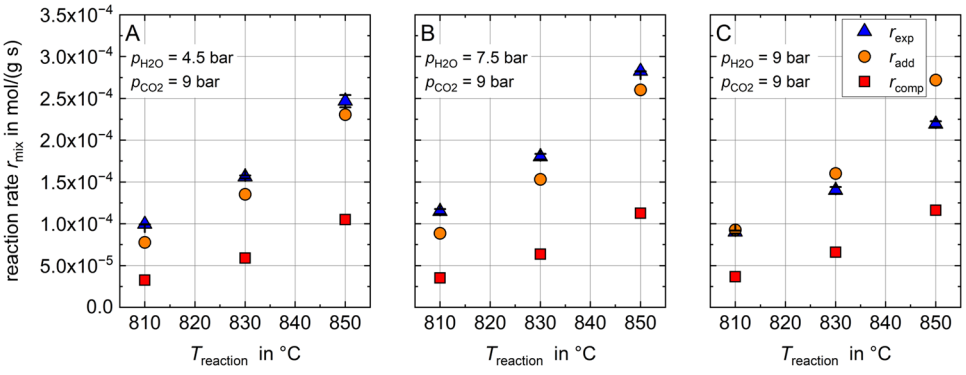

Figure 6. P1600: experimental reaction rates of mixed gasification r_{exp} with error bars for increasing H_2O partial pressures of 4.5 bar (A), 7.5 bar (B), and 9 bar (C) at a CO_2 partial pressure of 9 bar and at 810−850 °C versus additive and competitive models (r_{add} and r_{comp}).

https://doi.org/10.1021/acs.energyfuels.5c04287
Energy Fuels XXXX, XXX, XXX−XXX

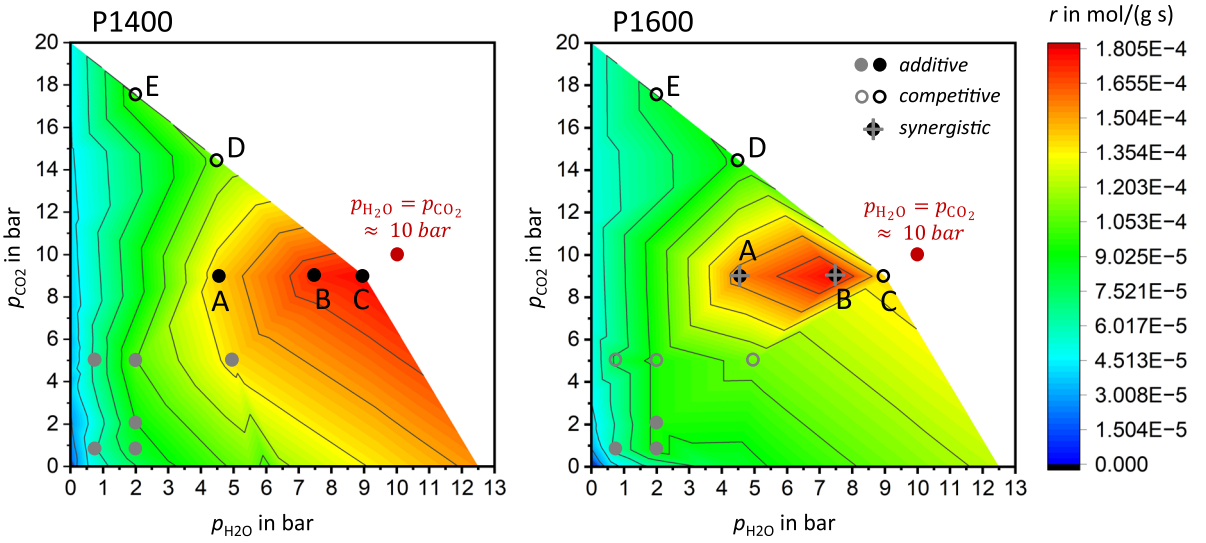

Figure 7. Heat maps of the experimentally derived reaction rates of mixed gasification r_{exp} for 830 °C (A−E) with PL kinetics for the heterogeneous water−gas reaction on the abscissa and PL (P1400) respectively LH (P1600) kinetics for the Boudouard reaction on the ordinate; the mechanism of interaction of H_2O and CO_2 found for each experiment is indicated by different symbols.

For char type P1600, having stronger graphitization, additive behavior was only found for low partial pressures of $p_{H_2O} \leq 2$ bar and $p_{CO_2} \leq 2$ bar (Figure 7) and explained by the inferior number of reactive sites per surface area. For $p_{CO_2} = 9$ bar and 4.5 bar $\leq p_{H_2O} \leq 7.5$ bar, synergistic behavior is dominant. The interaction passes back to competitive behavior again for $p_{CO_2} = 9$ bar and $p_{H_2O} = 9$ bar. Consequently, it can be inferred that the reaction rates at $p_{CO_2} \approx 10$ bar and $p_{H_2O} \approx 10$ bar lie between the predictions of the additive and competitive models and are lower than those observed for char type P1400.

With Figure 7 at $p_{H_2O} = 4.5$ bar, a decrease of the reaction rates with increasing CO_2 partial pressure from 9 to 14.5 bar (A to D) can be observed for both char types. This circumstance seems unintuitive at a first glance. However, when the interaction of H_2O and CO_2 passes to competition with increasing CO_2 partial pressure, the CO_2 molecules gradually displace H_2O molecules from reactive sites. The Boudouard reaction consequently becomes more dominant. As the Boudouard reaction is slower than the heterogeneous water−gas reaction, this leads to a decrease of the overall reaction rate. A more detailed analysis can be found in Section S.6.

During EFG, reaction temperatures are much higher than the temperatures investigated in the dFBR. At these temperatures, the effective reaction rate is limited by mass transport through the particles' pores. Due to pore diffusion limitation, gaseous reaction partners are consumed before they can penetrate deeper into the pores. Therefore, the reactive surface area deeper inside the pore network is less accessible, leading to an apparent reduction in the reactive surface area. Assuming that the reactive sites are equally distributed over the whole reactive surface area, surface saturation and the onset of competition should lie within the partial pressure ranges described in this work. Uncertainty remains due to the different diffusion behavior of H_2O and CO_2. H_2O molecules diffuse faster and have access to smaller pores. At higher temperatures, the accessible surface will decrease differently for both molecules, which is why estimating the reaction rate in the mixture can only be an approximation.

The temperature in the flame zone of the reactor[3] influences the severity of secondary pyrolysis of the chars. With higher temperatures of secondary pyrolysis, the chars are more strongly graphitized, leading to an inferior number of reactive sites per surface area. In turn, with less reactive sites, stronger competitive behavior was observed at technically relevant H_2O and CO_2 partial pressures. For the chars investigated in this work, additive behavior can be expected for lower temperatures of secondary pyrolysis up to around 1400 °C, while the competitive behavior results from higher temperatures of about 1600 °C.

The assumption of H_2O and CO_2 partial pressures of about 10 bar is a typical number for technical gasifiers operated at 40 bar and assuming that H_2O, H_2, CO_2 and CO are in equilibrium. This helps to define a target partial pressure range for kinetic analysis. The actual gas composition depends on the feed composition, the stoichiometric air ratio, the temperature in the reactor, and burner nozzle configuration, resulting in a spatial variation in gas composition.[3,58] Furthermore, besides H_2O and CO_2, also the product gases H_2 and CO are present with partial pressures of the same order of magnitude. Because of product gas inhibition, the reaction rates should be inferior, as can, for example, be seen by means of the Langmuir−Hinshelwood expression. Keller et al. investigated the product gas inhibition on coal gasification in mixtures of CO_2, H_2O, H_2, and CO in a pressurized drop-tube furnace (partial pressures up to 4 bar each). The reaction rates were successfully described with a competitive LH model.[4] This evokes the question after experimental assessment and kinetic modeling of product gas inhibition of the gasification of beech wood char at technically relevant partial pressures for entrained flow gasification.

https://doi.org/10.1021/acs.energyfuels.5c04287
Energy Fuels XXXX, XXX, XXX−XXX

4. SUMMARY AND CONCLUSION

The aim of this paper was to describe the gasification kinetics and the steam−CO_2 interaction of two beech wood char qualities for technically relevant atmospheres of entrained flow gasification, i.e., about 10 bar steam and CO_2 partial pressure each.

The char qualities of 50−100 μm were previously prepared by secondary pyrolysis of a primary beech wood char in a drop-tube reactor at 1400 and 1600 °C. The different severities of secondary pyrolysis led to different micropore surface areas, graphitization degrees, and dispersions of calcium on the char surface (Schneider et al., 2021a).

Gasification experiments were conducted in a pressurized differential fixed bed reactor at 810−870 °C. In a first step, steam gasification rates at H_2O partial pressures up to 12.5 bar were determined and the kinetics were modeled with a power law approach. In a second step, gasification experiments with mixed atmospheres, i.e., steam partial pressures between 2 and 9 bar and CO_2 partial pressures between 9 and 17.5 bar, were conducted. Experimental reaction rates were compared to the separate and shared reactive sites models. The pressurized CO_2 gasification kinetics of the beech wood char qualities were previously published (Schneider et al., 2021b) and were used to interpret the experimental results of this work.

Two key findings for beech wood char gasification at technically relevant H_2O partial pressures and technically relevant H_2O−CO_2 mixtures (for entrained flow gasification) can be summarized as below.

(1) Steam gasification at partial pressures up to 12.5 bar results in higher mass-specific reaction rates compared to CO_2 gasification at corresponding CO_2 partial pressures. This tendency is found in literature for coal char or biochar at low steam partial pressures. The reaction rates in H_2O are higher for the char with higher micro-porosity, a less ordered carbon matrix, and lower dispersion of calcium. Although it is not possible to isolate the effects of graphitization and calcium dispersion, the results suggest that a higher number of reactive sites per char surface (due to the lower degree of graphitization) and the larger micropore surface area are reflected in the higher preexponential factor. The activation energies of the heterogeneous water−gas reaction are comparable for both char types, suggesting similar reactive sites.

(2) The interaction of H_2O and CO_2 on the surface of beech wood char can in principle be described by additive behavior at low partial pressures and a transition to competitive behavior with increasing partial pressures. The transition from additive to competitive behavior most likely depends on the number of reactive sites per surface area and therefore on the degree of structural ordering of the carbon matrix (graphitization).

Consequently, it is concluded that for the technical application, the severity of secondary pyrolysis in the EFG reactor, which strongly influences the degree of graphitization and the microporosity, also plays a decisive role in the H_2O gasification rate and the interaction between H_2O and CO_2 being additive or competitive. For application in technical gasifiers, it is essential to first determine whether additive or competitive behavior is present, as this has a significant impact on the reaction rate.

In technical gasifiers, also the product gases CO and H_2 are present at high partial pressures. Uncertainty remains with respect to the influence of product gases on the transition from additive to competitive behavior. Therefore, future studies should also investigate the influence of product gases on the interactions of CO_2 and H_2O during gasification.

■ ASSOCIATED CONTENT

Supporting Information

The Supporting Information is available free of charge at https://pubs.acs.org/doi/10.1021/acs.energyfuels.5c04287.

Derivation of the Langmuir−Hinshelwood kinetics (S.1.), flow scheme of the differential fixed-bed reactor (dFBR) (S.2.), evolution of the conversion rate and product gas concentrations during gasification and impact of the deviation of the conversion rate from the UCM model behavior (S.3.), consistency with former research (S.4.), experimental reaction rates and reaction rates of the additive and competitive approach (S.5.), and classification of the gasification behavior (S.6.) (PDF)

■ AUTHOR INFORMATION

Corresponding Author

Stella Walker − *Karlsruhe Institute of Technology, Engler-Bunte-Institute, Fuel Technology, EBI-ceb, 76131 Karlsruhe, Germany*; orcid.org/0000-0003-2570-068X; Phone: +49 721 608 42563; Email: stella.walker@kit.edu

Author

Thomas Kolb − *Karlsruhe Institute of Technology, Engler-Bunte-Institute, Fuel Technology, EBI-ceb, 76131 Karlsruhe, Germany; Karlsruhe Institute of Technology, Institute for Technical Chemistry, ITC-vgt, 76344 Eggenstein-Leopoldshafen, Germany*

Complete contact information is available at: https://pubs.acs.org/10.1021/acs.energyfuels.5c04287

Author Contributions

S.W.: Conceptualization, methodology, investigation, formal analysis, software, validation, visualization, writing—original draft. T.K.: writing—review and editing, supervision.

Notes

The authors declare no competing financial interest.

■ ACKNOWLEDGMENTS

The authors gratefully acknowledge the financial support by the Helmholtz Association of German Research Centers (HGF), within the research program Energy Efficiency, Materials and Resources (EMR). Further acknowledgment goes to P. Moog (KIT) and L. Springmann (formerly KIT) for their experimental support.

■ SYMBOLS USED

E_A	activation energy, kJ/mol
k	rate constant for kinetic models, variable
k_0	preexponential factor for Arrhenius approach, variable
L_a	radial expansion of graphene layers, m
$\tilde{M}$	molar mass, g/mol
m	mass, g
$\dot{n}$	molar flow rate, mol/s
n	reaction order

https://doi.org/10.1021/acs.energyfuels.5c04287
Energy Fuels XXXX, XXX, XXX−XXX

p	pressure/partial pressure, bar
R	reactivity, 1/s
r	reaction rate, mol/(g s)
R_U	universal gas constant, J/(mol K)
t	time, s
T	temperature, K or °C
$\dot{V}$	volume flow, m^3/s
X	conversion

SUBSCRIPTS

add	additive approach
C	carbon
CO_2	CO_2 gasification atmosphere
comp	competitive approach
conv	converted
exp	experimentally determined
f	free reactive carbon center
gasif	gasified (total amount of gasified carbon)
H_2O	H_2O gasification atmosphere
i	refers to variable species (CO_2 or H_2O)
LH	Langmuir−Hinshelwood
molar	molar
PL	power law
reaction	gasification experiment
tot	total
UCM	uniform conversion model

ABBREVIATIONS

ad	air-dried
daf	dry ash free
dFBR	differential fixed bed reactor
EFG	entrained flow gasification
LH	Langmuir−Hinshelwood
PL	power law
P1400	beech wood char pyrolyzed at 1400 °C
P1600	beech wood char pyrolyzed at 1600 °C
UCM	uniform conversion model
wt.	weight

REFERENCES

(1) Riorda, A.; Negro, V.; Pantaleo, A. M.; Matteucci, F.; Shah, N.; Chiaramonti, D. Sustainable Hydrogen from Biomass: What Is Its Potential Contribution to the European Defossilization Targets? *Energy fuels* **2025**, *39* (13), 6412−6425.

(2) Fleck, S.; Santo, U.; Hotz, C.; Jakobs, T.; Eckel, G.; Mancini, M.; Weber, R.; Kolb, T. Entrained flow gasification Part 1: Gasification of glycol in an atmospheric-pressure experimental rig. *Fuel* **2018**, *217*, 306−319.

(3) Haas, M.; Dammann, M.; Fleck, S.; Kolb, T. Entrained flow gasification: Impact of fuel spray distribution on reaction zone structure. *Fuel* **2023**, *334*, No. 126572.

(4) Keller, F.; Küster, F.; Meyer, B. Determination of coal gasification kinetics from integral drop tube furnace experiments with steam and CO2. *Fuel* **2018**, *218*, 425−438.

(5) Li, F.; Yan, Q.; Huang, J.; Zhao, J.; Fang, Y.; Wang, J. Lignite-char gasification mechanism in mixed atmospheres of steam and CO 2 at different pressures. *Fuel Process. Technol.* **2015**, *138* (1), 555−563.

(6) Da Silva, J. C. G.; Alves, J. L. F.; Mumbach, G. D.; Andersen, S. L. F.; de Fatima Peralta Muniz Moreira, R.; Jose, H. J. Hydrogen-rich syngas production from steam gasification of Brazilian agroindustrial wastes in fixed bed reactor: kinetics, energy, and gas composition. *Biomass Conv. Bioref.* **2024**, *14*, 25901−25924.

(7) Gómez-Vásquez, R. D.; Camargo-Trillos, D. A.; Castiblanco, E. A.; Humánez, J.; Bula, A. Determination of intrinsic kinetic of corncob char gasification with CO2 and steam using multipore diffusion model. *Biomass Conv. Bioref.* **2024**, *14*, 14339−14351.

(8) Zhao, S.; Ding, L.; Ruan, Y.; Bai, B.; Qiu, Z.; Li, Z. Experimental and Kinetic Studies on Steam Gasification of a Biomass Char. *Energies* **2021**, *14* (21), No. 7229.

(9) Dahou, T.; Defoort, F.; Nguyen, H. N.; Bennici, S.; Jeguirim, M.; Dupont, C. Biomass steam gasification kinetics: Relative impact of char physical properties vs. inorganic composition. *Biomass Conv. Bioref.* **2022**, *12* (8), 3475−3490.

(10) Schneider, C.; Zeller, M.; Böhm, D.; Kolb, T. Influence of pressure on the gasification kinetics of two high-temperature beech wood chars with CO2, H2O and its mixture. *Fuel* **2021**, *299* (3), No. 120523.

(11) Guizani, C.; Escudero Sanz, F. J.; Salvador, S. Influence of temperature and particle size on the single and mixed atmosphere gasification of biomass char with H 2 O and CO 2. *Fuel Process. Technol.* **2015**, *134* (1), 175−188.

(12) Guizani, C.; Jeguirim, M.; Gadiou, R.; Escudero Sanz, F. J.; Salvador, S. Biomass char gasification by H2O, CO2 and their mixture: Evolution of chemical, textural and structural properties of the chars. *Energy* **2016**, *112* (6), 133−145.

(13) Feng, D.; Zhao, Y.; Zhang, Y.; Xu, H.; Zhang, L.; Sun, S. Catalytic mechanism of ion-exchanging alkali and alkaline earth metallic species on biochar reactivity during CO2/H2O gasification. *Fuel* **2018**, *212* (6), 523−532.

(14) Nilsson, S.; Gómez-Barea, A.; Ollero, P. Gasification of char from dried sewage sludge in fluidized bed: Reaction rate in mixtures of CO2 and H2O. *Fuel* **2013**, *105*, 764−768.

(15) Stoesser, P.; Schneider, C.; Kreitzberg, T.; Kneer, R.; Kolb, T. On the influence of different experimental systems on measured heterogeneous gasification kinetics. *Appl. Energy* **2018**, *211* (4), 582−589.

(16) Walker, S.; Kolb, T. Operation of a differential fixed bed reactor for investigations on micro-kinetics of heterogeneous gasification reactions. *Fuel* **2025**, *381*, No. 133561.

(17) Schneider, C.; Walker, S.; Phounglamcheik, A.; Umeki, K.; Kolb, T. Effect of calcium dispersion and graphitization during high-temperature pyrolysis of beech wood char on the gasification rate with CO2. *Fuel* **2021**, *283* (3), No. 118826.

(18) Rossberg, M.; Wicke, E. Transportvorgänge und Oberflächen-reaktionen bei der Verbrennung graphitischen Kohlenstoffs. *Chem. Ing. Tech.* **1956**, *28* (3), 181−189.

(19) Roberts, D. G.; Harris, D. J. Char Gasification Kinetics in Mixtures of CO 2 and H 2 O: The Role of Partial Pressure in Determining the Extent of Competitive Inhibition. *Energy Fuels* **2014**, *28* (12), 7643−7648.

(20) Roberts, D. G.; Harris, D. J. A Kinetic Analysis of Coal Char Gasification Reactions at High Pressures. *Energy Fuels* **2006**, *20* (6), 2314−2320.

(21) Laurendau, N. M. Heterogeneous Kinetics of Coal Char Gasification and Combustion. *Prog. Energy Combust. Sci.* **1978**, 221−270.

(22) Di Blasi, C. Combustion and gasification rates of lignocellulosic chars. *Prog. Energy Combust. Sci.* **2009**, *35* (2), 121−140.

(23) Kreitzberg, T.; Haustein, H. D.; Gövert, B.; Kneer, R. Investigation of Gasification Reaction of Pulverized Char Under N2/CO2 Atmosphere in a Small-Scale Fluidized Bed Reactor. *J. Energy Resour. Technol.* **2016**, *138* (4), No. 042207, DOI: 10.1115/1.4032791.

(24) Schneider, C.; Rincón Prat, S.; Kolb, T. Determination of active sites during gasification of biomass char with CO2 using temperature-programmed desorption. Part 1: Methodology & desorption spectra. *Fuel* **2020**, *267* (4), No. 116726.

(25) Du, Y.; Wang, C.; Xin, H.; Che, D.; Mathews, J. P. Competitive or additive behavior for H2O and CO2 gasification of coal char?: Exploration via simplistic atomistic simulation. *Carbon* **2019**, *141* (12), 226−237.

https://doi.org/10.1021/acs.energyfuels.5c04287
Energy Fuels XXXX, XXX, XXX−XXX

(26) Wang, Y.; Bell, D. A. Competition between H 2 O and CO 2 during the gasification of Powder River Basin coal. *Fuel* **2017**, *187* (7−8), 94−102.
(27) Chen, C.; Wang, J.; Liu, W.; Zhang, S.; Yin, J.; Luo, G.; Yao, H. Effect of pyrolysis conditions on the char gasification with mixtures of CO2 and H2O. *Proc. Combust. Inst.* **2013**, *34* (2), 2453−2460.
(28) Chen, C.; Zhang, S.; Xu, K.; Luo, G.; Yao, H. Experimental and Modeling Study of Char Gasification with Mixtures of CO 2 and H 2 O. *Energy Fuels* **2016**, *30* (3), 1628−1635.
(29) Zhang, R.; Wang, Q. H.; Luo, Z. Y.; Fang, M. X.; Cen, K. F. Competition and Inhibition Effects during Coal Char Gasification in the Mixture of H 2 O and CO 2. *Energy Fuels* **2013**, *27* (9), 5107−5115.
(30) Roberts, D. G.; Harris, D. J. Char gasification in mixtures of CO2 and H2O: Competition and inhibition. *Fuel* **2007**, *86* (17−18), 2672−2678.
(31) Umemoto, S.; Kajitani, S.; Hara, S. Modeling of coal char gasification in coexistence of CO2 and H2O considering sharing of active sites. *Fuel* **2013**, *103*, 14−21.
(32) Zhang, R.; Chen, Y.; Lei, K.; Liu, D. The effects of specific surface area and ash on char gasification mechanisms in the mixture of H2O, CO2, H2 and CO. *Fuel* **2017**, *209*, 109−116.
(33) Gao, M.; Yang, Z.; Wang, Y.; Bai, Y.; Li, F.; Xie, K. Impact of calcium on the synergistic effect for the reactivity of coal char gasification in H 2 O/CO 2 mixtures. *Fuel* **2017**, *189*, 312−321.
(34) Tagutchou, J. P.; van de steene, L.; Escudero Sanz, F. J.; Salvador, S. Gasification of Wood Char in Single and Mixed Atmospheres of H 2 O and CO 2. *Energy Sources, Part A* **2013**, *35* (13), 1266−1276.
(35) Bai, Y.; Lv, P.; Yang, X.; Gao, M.; Zhu, S.; Yan, L.; Li, F. Gasification of coal char in H2O/CO2 atmospheres: Evolution of surface morphology and pore structure. *Fuel* **2018**, *218*, 236−246.
(36) Zoulalian, A.; Bounaceur, R.; Dufour, A. Kinetic modelling of char gasification by accounting for the evolution of the reactive surface area. *Chem. Eng. Sci.* **2015**, *138*, 281−290.
(37) Pflieger, C.; Lotz, K.; Hilse, N.; Berger, C. M.; Schiemann, M.; Debiagi, P.; Hasse, C.; Scherer, V.; Muhler, M. Catalytic influence of mineral compounds on the reactivity of cellulose-derived char in O2-, CO2-, and H2O-containing atmospheres. *Fuel* **2021**, *287* (1700−1729), No. 119584.
(38) Hurt, R.; Sun, J.-K.; Lunden, M. A Kinetic Model of Carbon Burnout in Pulverized Coal Combustion. *Combust. Flame* **1998**, *113* (113), 181−197.
(39) Tremel, A.; Spliethoff, H. Gasification kinetics during entrained flow gasification − Part II: Intrinsic char reaction rate and surface area development. *Fuel* **2013**, *107*, 653−661.
(40) Senneca, O.; Ontyd, C.; Cerciello, F.; Schiemann, M.; Scherer, V. Extension of the Thermal Annealing Concepts Developed for Coal Combustion to Conversion of Lignocellulosic Biomass. *Energy Fuels* **2020**, *34* (3), 3661−3670.
(41) Naim, W.; Treu, P.; Dohrn, M.; Saraçi, E.; Grunwaldt, J.-D.; Fendt, S.; Spliethoff, H. Structure-Reactivity- and Modelling-Relationships during Thermal Annealing in Biomass Entrained-Flow Gasification: The Effect of Temperature and Residence Time. *Fuel* **2025**, *383*, No. 133848.
(42) Bouraoui, Z.; Dupont, C.; Jeguirim, M.; Limousy, L.; Gadiou, R. CO2 gasification of woody biomass chars: The influence of K and Si on char reactivity. *C. R. Chim.* **2016**, *19* (4), 457−465.
(43) Dupont, C.; Jacob, S.; Marrakchy, K. O.; Hognon, C.; Grateau, M.; Labalette, F.; Da Silva Perez, D. How inorganic elements of biomass influence char steam gasification kinetics. *Energy* **2016**, *109* (4), 430−435.
(44) Yip, K.; Tian, F.; Hayashi, J.; Wu, H. Effect of Alkali and Alkaline Earth Metallic Species on Biochar Reactivity and Syngas Compositions during Steam Gasification †. *Energy Fuels* **2010**, *24* (1), 173−181.
(45) Vassilev, S. V.; Baxter, D.; Andersen, L. K.; Vassileva, C. G. An overview of the chemical composition of biomass. *Fuel* **2010**, *89* (5), 913−933.
(46) Kopyscinski, J.; Rahman, M.; Gupta, R.; Mims, C. A.; Hill, J. M. K2CO3 catalyzed CO2 gasification of ash-free coal. Interactions of the catalyst with carbon in N2 and CO2 atmosphere. *Fuel* **2014**, *117*, 1181−1189.
(47) Aho, A.; DeMartini, N.; Pranovich, A.; Krogell, J.; Kumar, N.; Eränen, K.; Holmbom, B.; Salmi, T.; Hupa, M.; Murzin, D. Y. Pyrolysis of pine and gasification of pine chars—influence of organically bound metals. *Bioresour. Technol.* **2013**, *128*, 22−29.
(48) Perander, M.; DeMartini, N.; Brink, A.; Kramb, J.; Karlström, O.; Hemming, J.; Moilanen, A.; Konttinen, J.; Hupa, M. Catalytic effect of Ca and K on CO2 gasification of spruce wood char. *Fuel* **2015**, *150*, 464−472.
(49) Elsaddik, M.; Nzihou, A.; Delmas, M.; Delmas, G.-H. Steam gasification of cellulose pulp char: Insights on experimental and kinetic study with a focus on the role of Silicon. *Energy* **2023**, *271*, No. 126997.
(50) Liu, R.; Zhang, Y.; Ling, Z.; Song, Y. Some new insights into the synergy occurring during char gasification in CO2/H2O mixtures. *Fuel* **2020**, *268*, No. 117307.
(51) Yu, G.; Yu, D.; Liu, F.; Yu, X.; Han, J.; Wu, J.; Xu, M. Different catalytic action of ion-exchanged calcium in steam and CO2 gasification and its effects on the evolution of char structure and reactivity. *Fuel* **2019**, *254* (12−13), No. 115609.
(52) Fatehi, H.; Bai, X.-S. Structural evolution of biomass char and its effect on the gasification rate. *Appl. Energy* **2017**, *185*, 998−1006.
(53) Tarlinski, D.; Freisewinkel, E.; Eisenbach, T.; Span, R.; Schiemann, M.; Scherer, V. Combustion of single walnut shell particles in a laminar flow reactor under oxy-fuel conditions: Optical measurements and particle sampling. *Fuel* **2024**, *369*, No. 131613.
(54) Wedler, C.; Span, R. A pore-structure dependent kinetic adsorption model for consideration in char conversion − Adsorption kinetics of CO2 on biomass chars. *Chem. Eng. Sci.* **2021**, *231* (11), No. 116281.
(55) Dammann, M. *Numerical modelling and simulation of atmospheric entrained flow gasification of surrogate fuels*; Karlsruher Institut für Technologie (KIT), 2024 DOI: 10.5445/IR/1000172116.
(56) Higman, C.; van der Burgt, M. *Gasification*; Elsevier, 2003.
(57) Dahou, T.; Defoort, F.; Khiari, B.; Labaki, M.; Dupont, C.; Jeguirim, M. Role of inorganics on the biomass char gasification reactivity: A review involving reaction mechanisms and kinetics models. *Renewable Sustainable Energy Rev.* **2021**, *135*, No. 110136.
(58) Dammann, M.; Santo, U.; Böning, D.; Knoch, H.; Eberhard, M.; Kolb, T. Entrained flow gasification: Pilot-scale experimental, balancing and equilibrium data for model validation. *Fuel* **2025**, *382*, No. 132809.

https://doi.org/10.1021/acs.energyfuels.5c04287
Energy Fuels XXXX, XXX, XXX−XXX